Journal of Sound and Vibration 496 (2021) 115932

Contents lists available at ScienceDirect

Journal of Sound and Vibration

journal homepage: www.elsevier.com/locate/jsv

A novel structural damage identification approach using damage-induced perturbation in longitudinal vibration ☆

Wei Xu [a], Weidong Zhu [b,*], Zhongqing Su [c], Maosen Cao [a], Hao Xu [d]

[a] Department of Engineering Mechanics, Hohai University, Nanjing 210098, People's Republic of China
[b] Department of Mechanical Engineering, University of Maryland, Baltimore County, Baltimore, MD 21250, United States
[c] Department of Mechanical Engineering, The Hong Kong Polytechnic University, Hung Hom, Kowloon, Hong Kong, People's Republic of China
[d] School of Aeronautics and Astronautics, Faculty of Vehicle Engineering and Mechanics, State Key Laboratory of Structural Analysis for Industrial Equipment, Dalian University of Technology, Dalian 116024, People's Republic of China

ARTICLE INFO

Article history:
Received 27 September 2020
Revised 19 December 2020
Accepted 4 January 2021
Available online 5 January 2021

Keywords:
Structural damage identification
Longitudinally vibrating structure
Vibration shape
Axial pseudo-force
Three-dimensional laser scanning measurement

ABSTRACT

Structural damage identification approaches relying on structural vibration shapes (VSs) have been widely developed. Among the approaches, the pseudo-force approach has attracted increasing attention during the recent decade owing to the fact that the damage-induced pseudo-force is concentrated within the damage region only and rapidly attenuates at undamaged locations. Transverse pseudo-forces (TPFs) relying on flexural VSs have been used for structural damage identification. However, the TPF approach is inapplicable to some structures governed mainly by tension and not bending, such as cables in a cable-stayed bridge, because bending effects on their flexural vibrations are much smaller compared to their tension effects. In contrast, longitudinal VSs can be useful for identifying such damages, although they are much more difficult to measure than flexural VSs. In this study, a new concept of axial pseudo-force (APF) is formulated using damage-induced perturbation in longitudinal vibration, which forms the basis of a novel damage identification approach for longitudinally vibrating structures. Unlike the TPF approach relying on transverse bending, the proposed APF approach relies on axial tension/compression. In particular, a damage index (DI) is established to indicate and locate structural damage. The multiscale analysis is integrated into the DI to enhance its robustness against environmental noise interference. A normalization strategy is further proposed to deal with unknown material and structural parameters in practical scenarios. The capability of the approach in identifying damage in longitudinally vibrating structures is analytically verified on bars with two-sided notches. The applicability of the approach is experimentally validated by identifying a two-sided notch in an aluminum bar whose longitudinal VSs were acquired through non-contact vibration measurement using a three-dimensional (3D) scanning laser vibrometer (SLV).

© 2021 Elsevier Ltd. All rights reserved.

☆ Handling Editor: Dr E Chatzi.
* Corresponding author.
E-mail addresses: wxu@hhu.edu.cn (W. Xu), wzhu@umbc.edu (W. Zhu), zhongqing.su@polyu.edu.hk (Z. Su), cmszhy@hhu.edu.cn (M. Cao), xuhao@dlut.edu.cn (H. Xu).

https://doi.org/10.1016/j.jsv.2021.115932
0022-460X/© 2021 Elsevier Ltd. All rights reserved.

1. Introduction

Structural damage identification methods relying on vibration have been widely developed during the recent decades [1–5]. Structural vibration shapes (VSs), including mode shapes (MSs) and steady-state response shapes under harmonic excitation (SRSHEs), have been increasingly used for damage identification [6].

For damage in a beam with reduced cross-sectional dimensions, such as a notch or crack, it reduces both its bending stiffness and axial stiffness in the damage region, leading to discontinuities in derivatives of its flexural and longitudinal VSs, respectively [7]. Thereby, the damage can be identified by local discontinuities in derivatives of VSs. Derivatives of flexural VSs of beams have been commonly used for identification of local damages, examples of damage indicators being curvature [8–19], strain energy [20–22], Teager-Kaiser energy [23–25], and wavelet transform [26–29], in which damage-induced local discontinuities have been used to indicate and locate damage if there are no significant changes in global trends of the indicators. However, for initial damages whose locations are closely spaced, the structures need to be densely sampled with small intervals, which results in interference caused by noise components in VSs that can be significantly amplified due to numerical evaluation of differentiation in the damage indicators, the most common example being the second-order differentiation in curvatures [23]; on the other hand, as local stiffness and/or mass changes caused by initial damage are small [2], unobvious local discontinuities of derivatives of flexural VSs can be obscured by fluctuant global trends [10–13]. In those situations, local changes in derivatives of flexural VSs become ambiguous for damage identification and can provide misleading results.

In recent years, the pseudo-force approach is developed and has attracted increasing attention [30–38]. As the pseudo-force is generated only by the damage and is free of effects from fluctuant global trends, it is capable of identifying initial damage. By rearranging perturbation in an equation of motion that is induced by damage-caused changes in local stiffness/mass, effect of local damage can be regarded as an equivalent force applied on structural elements bearing damage, referred to as a “pseudo-force” or “pseudo-excitation”. Theoretically, the pseudo-force exists in the damage region only and vanishes at undamaged locations, in the form of a Heaviside step function whose expression for this study is given in Section 2.1. In practice, pseudo-forces cannot completely vanish at undamaged locations due to uncertainties during measurements; instead, they rapidly attenuate at undamaged locations. Thereby, the occurrence, location, and size of the initial damage can be characterized by peaks of pseudo-forces. Representative studies of damage identification of beams using transverse pseudo-forces (TPFs) are as follows. Inspired by the idea of reconstructing distribution of excitation forces applied on beams [39], Xu et al. [30] proposed a novel inverse approach for damage identification using local perturbation to equilibrium characteristics of beam components, whereby a through-width notch in an aluminum beam was identified. A low-pass wavenumber filtering was proposed for denoising, with an aim of dealing with noise contamination in measured MSs. With the same concern about noise interference, Cao et al. [31] proposed a new concept of multiscale pseudo-force by transforming the pseudo-force into the wavelet domain. The multiscale nature brought additional benefits to enhance robustness of the approach against noise interference. Furthermore, to make the approach suitable for beams with unknown material and structural parameters, an optimization strategy for evaluating the constant related to the vibration frequency and material and structural parameters was integrated into the multi-scale pseudo-force [32]. Xu et al. [33] established a debonding index by reconstructing distribution of interfacial forces of a steel-reinforced concrete slab, whereby debonding-induced local perturbation to the structural dynamic equilibrium can be canvassed. Furthermore, a hybrid data fusion algorithm was proposed for identification of multiple debonding. Xu et al. [34] established the “weak formulation” of the pseudo-excitation approach by introducing weighted integration, whereby noise immunity of the pseudo-excitation approach can be enhanced. Multiple cracks were localized in an aluminum beam-type structure in a noisy condition using the enhanced pseudo-excitation approach. To locate damage in sub-regions that are divided from an entire beam component, “virtual vibration deflections” of sub-structures undergoing independent vibration were used for damage identification [35]. The enhanced pseudo-excitation approach was further developed, which is suitable for damage identification using curvature/strain signals [36]. In particular, a reconstruction strategy was proposed to derive vibration displacements through integration in the spatial domain. By means of the weak formulation, Zhang et al. [37] proposed a damage detection method based on virtual element boundary measurements. A novel local specific stiffness identification method was proposed based on a multiscale weak formulation [38]. Influences of key parameters, such as measurement interval, scale factor, and derivative order of measured vibration displacements, were investigated. Experimental validation was carried out on a beam with local reduction in thickness.

Although the TPF approach relying on flexural VSs has been developed, it is inapplicable to some structures governed mainly by tension and not bending, such as cables in a cable-stayed bridge, because bending effects on their flexural vibrations are much smaller compared to their tension effects. In contrast, longitudinal VSs can be useful for identifying damages in such structures, although they are much more difficult to measure than flexural VSs. In the recent decade, the non-contact vibration measurement technique using a three-dimensional (3D) scanning laser vibrometer (SLV) has been developed to accurately acquire densely sampled longitudinal VSs [6]. By addressing the inapplicability of the TPF approach to tension-governed structures, a new concept of axial pseudo-force (APF) is formulated in this study using damage-induced perturbation in longitudinal vibration, which forms the basis of a novel damage identification approach for longitudinally vibrating structures. Unlike the TPF approach relying on transverse bending, the proposed APF approach relies on axial tension/compression. The APF approach is applied in this study to bar-type structures for damage identification. It can be extended to other longitudinally vibrating structures such as cables in a cable-stayed bridge in some future study.

The rest of this paper is organized as follows. Section 2 formulates a new concept of APF, by which a damage index (DI) is established to indicate and locate damage in longitudinally vibrating structures. Superior to the existing TPF approach, the proposed APF approach is useful for damage identification in tension-governed structures. In particular, the multiscale analysis is integrated into the DI to enhance its robustness against environmental noise interference. A normalization strategy is further proposed to deal with unknown material and structural parameters in practical scenarios. Section 3 analytically verifies the capability of the APF approach on bars with two-sided notches and single-sided cracks. Section 4 experimentally validates the applicability of the approach by identifying a two-sided notch in an aluminum bar. The bar is excited by an electromagnetic shaker, and its longitudinal VSs are acquired through non-contact vibration measurement using a 3D SLV. Section 5 presents concluding remarks.

2. Damage identification of bars using APFs

2.1. APFs in bars

For a uniform intact bar under axial excitation, its equation of longitudinal motion can be expressed as [40]

$$AE\frac{\partial^2 u(x,t)}{\partial x^2} - \rho A\frac{\partial^2 u(x,t)}{\partial t^2} = f(x,t), \tag{1}$$

where $u(x,t)$ is the longitudinal displacement of the bar, x is the spatial position along its length, t is time, E is the elastic modulus, A is the cross-sectional area, ρ is the mass density, and $f(x,t)$ is the distributed axial excitation force. By assuming that a damage, *e.g.*, a notch, crack, or inner defect, is introduced into the uniform intact bar, spanning from $x = x_1$ to $x = x_2$ along its length, its elastic modulus, cross-sectional area, and mass density can be represented as

$$E(x) = \begin{cases} E^I & x \notin [x_1, x_2] \\ E^D(x) & x \in [x_1, x_2] \end{cases}, \tag{2a}$$

$$A(x) = \begin{cases} A^I & x \notin [x_1, x_2] \\ A^D(x) & x \in [x_1, x_2] \end{cases}, \tag{2b}$$

$$\rho(x) = \begin{cases} \rho^I & x \notin [x_1, x_2] \\ \rho^D(x) & x \in [x_1, x_2] \end{cases}, \tag{2c}$$

respectively, where E^I and $E^D(x)$ are elastic moduli at the intact and damaged locations, respectively, A^I and $A^D(x)$ are cross-sectional areas at intact and damaged locations, respectively, and $\rho^I$and $\rho^D(x)$ are mass densities at intact and damaged locations, respectively. Note that E^I, A^I, and ρ^I are assumed to be constant in the intact bar.

Substituting Eq. (2) into Eq. (1) yields

$$A^I E^I\frac{\partial^2 u(x,t)}{\partial x^2} - \rho^I A^I\frac{\partial^2 u(x,t)}{\partial t^2} = f(x,t) + f_{APF}(x,t), \tag{3}$$

where $f_{APF}(x,t)$ denotes the APF that is the equivalent axial force caused by the damage, applied at the damaged location from $x = x_1$ to $x = x_2$ along the bar:

$$f_{APF}(x,t) = \begin{cases} 0 & x \notin [x_1, x_2] \\ \left[E^I A^I - E^D(x)A^D(x)\right]\frac{\partial^2 u(x,t)}{\partial x^2} - \left[\rho^I A^I - \rho^D(x)A^D(x)\right]\frac{\partial^2 u(x,t)}{\partial t^2} & x \in (x_1, x_2) \end{cases}. \tag{4}$$

Eq. (3) indicates that the forced vibration of the damaged bar as governed by Eq. (1) is equivalent to the vibration of an intact bar under the combination of the axial external excitation and APF. A schematic of the APF applied on a bar element with a damage in it is illustrated in Fig. 1.

As the APF reflects damage-induced perturbation in the longitudinal vibration of the bar element, a damage identification approach using the APF can be established: Eq. (4) indicates that the APF is concentrated within the damage region and rapidly attenuates at undamaged locations, by which phenomenon damage can be indicated and located.

Consider that a pointwise axial excitation is applied at a specific location outside an inspection region of the bar. With regard to bar elements bearing no axial excitation, *i.e.*, $f(x,t) = 0$, Eq. (3) becomes

$$A^I E^I\frac{\partial^2 u(x,t)}{\partial x^2} - \rho^I A^I\frac{\partial^2 u(x,t)}{\partial t^2} = f_{APF}(x,t). \tag{5}$$

By assuming that the bar is undamped, its longitudinal MSs, denoted as $U_M(x)$, can be obtained by assuming that $u(x,t) = U_M(x)\sin(\omega_n t)$, where ω_n denotes an undamped longitudinal natural frequency of the bar. One can also assume that $u(x,t) = U_S(x)\sin(\omega t)$, where $U_S(x)$ denotes the longitudinal SRSHE of the bar at an excitation frequency ω that excludes an undamped longitudinal natural frequency [41]. Note that each VS in this study is associated with one vibration frequency: a MS is associated with the corresponding natural frequency and a SRSHE is associated with the harmonic excitation frequency for the steady-state vibration. Substituting the $u(x,t)$ expression in either case into Eq. (5) yields

$$A^I E^I\frac{\mathrm{d}^2 U(x)}{\mathrm{d}x^2} + \omega^2 \rho^I A^I U(x) = F_{APF}(x), \tag{6}$$

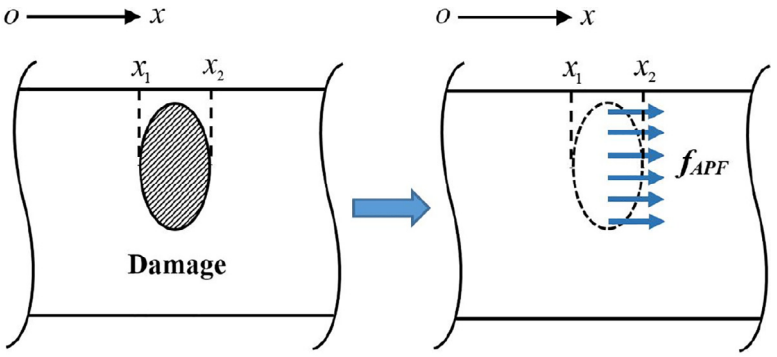

Fig. 1. Schematic of the APF applied on a bar element with a damage in it.

where $U(x)$ is the longitudinal VS that can be either the longitudinal MS $U_M(x)$ or the longitudinal SRSHE $U_S(x)$, and $F_{APF}(x)$ denotes the amplitude of $f_{APF}(x,t)$:

$$F_{APF}(x)=\begin{cases}0 & x\notin[x_1,x_2]\\ \left[E^IA^I-E^D(x)A^D(x)\right]\frac{\mathrm{d}^2U(x)}{\mathrm{d}x^2}+\omega^2\left[\rho^IA^I-\rho^D(x)A^D(x)\right]U(x) & x\in(x_1,x_2)\end{cases}. \tag{7}$$

Eq. (7) indicates that the amplitude of the APF is proportional to reductions of the elastic modulus, cross-sectional area, and mass density of the bar at the damage location. Thereby, a DI, denoted as *DI*, is established using the absolute value of F_{APF}, by which the occurrence, location, and extent of the damage can be characterized:

$$DI(x)=|F_{APF}(x)|=\left|A^IE^I\frac{\mathrm{d}^2U(x)}{\mathrm{d}x^2}+\omega^2\rho^IA^IU(x)\right|. \tag{8}$$

For flexural vibration, discontinuity peaks in amplitudes of TPFs appear at damage boundaries to indicate and locate the damage, the mechanism of which can be found in Ref. [30]. Similarly, for longitudinal vibration, the APF proposed in this study can reflect damage-induced discontinuities at damage boundaries. The continuity condition of the axial force at one edge of the damage ($x=x_1$) can be expressed as

$$\lim_{\varepsilon\to0}\left\{A^IE^I\frac{\mathrm{d}U(x_1-\varepsilon)}{\mathrm{d}x}\right\}=\lim_{\varepsilon\to0}\left\{A^D(x_1)E^D(x_1)\frac{\mathrm{d}U(x_1+\varepsilon)}{\mathrm{d}x}\right\}=F(x_1), \tag{9}$$

where ε is a small positive parameter and $F(x_1)$ denotes the amplitude of the axial force at $x=x_1$. By Eq. (9), one can obtain

$$\lim_{\varepsilon\to0}\left\{\frac{\mathrm{d}U(x_1-\varepsilon)}{\mathrm{d}x}\right\}=\frac{1}{A^IE^I}F(x_1), \tag{10a}$$

$$\lim_{\varepsilon\to0}\left\{\frac{\mathrm{d}U(x_1+\varepsilon)}{\mathrm{d}x}\right\}=\frac{1}{A^D(x_1)E^D(x_1)}F(x_1). \tag{10b}$$

Subtracting Eq. (10a) from Eq. (10b) yields

$$\lim_{\varepsilon\to0}\left\{\frac{\mathrm{d}U(x_1+\varepsilon)}{\mathrm{d}x}-\frac{\mathrm{d}U(x_1-\varepsilon)}{\mathrm{d}x}\right\}=\left(\frac{1}{A^D(x_1)E^D(x_1)}-\frac{1}{A^IE^I}\right)F(x_1). \tag{11}$$

By differentiating Eq. (11), $A^IE^I\frac{\mathrm{d}^2U(x_1)}{\mathrm{d}x^2}$ can be expressed as

$$\begin{aligned}A^IE^I\frac{\mathrm{d}^2U(x_1)}{\mathrm{d}x^2}&=A^IE^I\lim_{\varepsilon\to0}\left\langle\frac{1}{2\varepsilon}\left\{\frac{\mathrm{d}U(x_1+\varepsilon)}{\mathrm{d}x}-\frac{\mathrm{d}U(x_1-\varepsilon)}{\mathrm{d}x}\right\}\right\rangle\\&=A^IE^I\left(\frac{1}{A^D(x_1)E^D(x_1)}-\frac{1}{A^IE^I}\right)F(x_1)\lim_{\varepsilon\to0}\left(\frac{1}{2\varepsilon}\right)\\&=\left(\frac{A^IE^I}{A^D(x_1)E^D(x_1)}-1\right)F(x_1)\lim_{\varepsilon\to0}\left(\frac{1}{2\varepsilon}\right)\\&=\frac{1}{2}\left(\frac{A^IE^I}{A^D(x_1)E^D(x_1)}-1\right)F(x_1)\delta(x-x_1),\end{aligned} \tag{12a}$$

where $\delta(\cdot)$ denotes the Dirac delta function. Similarly, at the other edge of the damage ($x = x_2$), $A^I E^I \frac{\mathrm{d}^2 U(x_2)}{\mathrm{d}x^2}$ can be expressed as

$$\begin{aligned} A^I E^I \frac{\mathrm{d}^2 U(x_2)}{\mathrm{d}x^2} &= A^I E^I \lim_{\varepsilon \to 0} \left\langle \frac{1}{2\varepsilon} \left\{ \frac{\mathrm{d}U(x_2+\varepsilon)}{\mathrm{d}x} - \frac{\mathrm{d}U(x_2-\varepsilon)}{\mathrm{d}x} \right\} \right\rangle \\ &= A^I E^I \left(\frac{1}{A^I E^I} - \frac{1}{A^D(x_2) E^D(x_2)} \right) F(x_2) \lim_{\varepsilon \to 0} \left(\frac{1}{2\varepsilon} \right) \\ &= \left(1 - \frac{A^I E^I}{A^D(x_2) E^D(x_2)} \right) F(x_2) \lim_{\varepsilon \to 0} \left(\frac{1}{2\varepsilon} \right) \\ &= \frac{1}{2} \left(1 - \frac{A^I E^I}{A^D(x_2) E^D(x_2)} \right) F(x_2) \delta(x - x_2). \end{aligned} \tag{12b}$$

Hence, the DI can be rewritten as a Heaviside step function:

$$DI = \begin{cases} 0 & x \notin [x_1, x_2] \\ \left| \frac{1}{2} \left(\frac{A^I E^I}{A^D(x_1) E^D(x_1)} - 1 \right) F(x_1) \delta(x - x_1) + \omega^2 \rho^I A^I U(x_1) \right| & x = x_1 \\ \left| \frac{1}{2} \left(1 - \frac{A^I E^I}{A^D(x_2) E^D(x_2)} \right) F(x_2) \delta(x - x_2) + \omega^2 \rho^I A^I U(x_2) \right| & x = x_2 \\ \left| \left[E^I A^I - E^D(x) A^D(x) \right] \frac{\mathrm{d}^2 U(x)}{\mathrm{d}x^2} + \omega^2 \left[\rho^I A^I - \rho^D(x) A^D(x) \right] U(x) \right| & x \in (x_1, x_2) \end{cases}. \tag{13}$$

Eq. (13) indicates that in theory the DI exists within the damage region only and vanishes at undamaged locations; meanwhile, discontinuity peaks in the DI sharply rise at damage boundaries, *e.g.*, notch edges, whereas values of the DI within the damage region are expected to be much less pronounced. Thereby, the analytical mechanism for having discontinuity peaks in a DI at damage boundaries is explicitly expounded. Accordingly, discontinuity peaks in the DI can be used to indicate and locate damage: the exact location and size of the damage can be estimated by the locations of the discontinuity peaks in the DI. In contrast, the existing TPF approach can have limitations when it is applied to tension-governed structures. In those cases, damage-induced discontinuity peaks can be barely identified by the TPF approach because damage-induced bending perturbation in their flexural vibration equations can be negligible. Note that the discrete form of a DI $DI[x]$ can be obtained from the measured discrete VS $U[x]$, whose second-order derivative can be calculated by the finite difference method:

$$\frac{\mathrm{d}^2 U}{\mathrm{d}x^2}[x] = \frac{U[x-1] - 2U[x] + U[x+1]}{h_x^2}, \tag{14}$$

where h_x is the sampling interval.

2.2. Robustness against noise interference

As noise components are inevitably involved in measured VSs and can be amplified by second-order differentiation $\frac{\mathrm{d}^2}{\mathrm{d}x^2}$ involved in Eq. (8), actual damage-induced peaks in a DI can be masked by intense noise interference. By addressing this problem, robustness of the DI against noise interference is enhanced by multiscale analysis [42]. In this study, measured longitudinal VSs are inspected in a "region-by-region" manner [34] instead of the conventional "point-by-point" manner: the VSs are averaged in a scaled Gaussian windowing function $\bar{g}_s(x)$ that slides along VS signals:

$$\bar{U}(v, s) = \frac{1}{\sqrt{s}} U \otimes \bar{g}_s(v), \tag{15a}$$

$$U_s(x) = \bar{U}(v, s)\big|_{v=x}, \tag{15b}$$

where $\bar{g}_s(x) = \frac{1}{\sqrt{s}} g(\frac{-x}{s})$ with the Gaussian function $g(x) = (2/\pi)^{1/4} e^{-x^2}$ and scale parameter s, and $\otimes$ denotes convolution. It is noteworthy that unlike the pointwise U, U_s is represented in a scaled Gaussian window to average random noise. Eq. (15) produces a multiscale longitudinal VS U_s. Then, the multiscale DI (MDI), denoted as DI_s, can be obtained by replacing U with U_s in Eq. (8):

$$DI_s(x) = \left| A^I E^I \frac{\mathrm{d}^2 U_s(x)}{\mathrm{d}x^2} + \omega^2 \rho^I A^I U_s(x) \right|. \tag{16}$$

Thereby, the MDI exhibits an intrinsic multiscale property, which has two merits [42]. On the one hand, noise components caused by sensors and environments are inevitably involved in the measured longitudinal VSs. By gradually increasing scale

parameters, noise components are averaged in ever-wider Gaussian windows, leading to increasingly smooth second-order derivatives of VSs, which is demonstrated in Section 3.3. When scale parameters increase to satisficing levels, second-order derivatives of VSs become smooth enough, which means noise components in the VSs are basically eliminated. On the other hand, damage-induced discontinuity peaks at damage boundaries are naturally retained with increasing scale parameters, with which damage can be indicated and located. Thereby, the MDI is capable of identifying damage in longitudinally vibrating structures in noisy conditions using their longitudinal VSs. Note that the APF approach is an offline approach and noise interference needs to be eliminated by postprocessing measured VSs using multiscale analysis; for online damage identification, approaches based on Kalman filter [43], band-pass filters [44], and eigen-perturbation [5] are capable of removing noise components in VS data streams in real time.

2.3. Independence of material and structural parameters

Although the principle of damage identification using the APF is simple and straightforward, accurate baseline information, including vibration frequencies and material and structural parameters of longitudinally vibrating structures under inspection, needs to be known, which inhibits its applications to real-world structures whose material and structural parameters are unknown in most scenarios. By addressing this problem, a normalization strategy is proposed by dividing both sides of Eq. (8) by $A^I E^I$; one then has a normalized MDI (NMDI), denoted as DI_S^*:

$$DI_s^*(x) = \left| \frac{\mathrm{d}^2 U_s(x)}{\mathrm{d}x^2} + \lambda^2 U_s(x) \right|, \tag{17}$$

where $\lambda^2 = \frac{\omega^2 \rho^I}{E^I}$ is a constant related to the vibration frequency and material and structural parameters of a bar. However, as material and structural parameters of a longitudinally vibrating structure under inspection are usually unknown, the constant λ^2 cannot be directly obtained. By addressing this problem, λ^2 is evaluated in this study in a statistical manner instead of being directly evaluated [45]: first, a concept of pointwise constant $\lambda^2[x]$ for each measurement point in a VS is proposed. As DI_S^* in Eq. (17) rapidly attenuates and almost vanishes at undamaged locations of the structure, $\lambda^2[x]$ at undamaged locations can be alternatively calculated by Eq. (17) using $U_S[x]$:

$$\lambda^2[x] = -\frac{\mathrm{d}^2 U_s}{\mathrm{d}x^2}[x]/U_s[x]. \tag{18}$$

Second, as undamaged locations account for a great proportion of the inspection region, the pointwise constant $\lambda^2[x]$ with the maximum probability is regarded as the constant λ^2. Thereby, DI_S^* can be obtained by Eq. (17). By the statistical manner of evaluating λ^2, the APF approach becomes independent of the vibration frequency and material and structural parameters.

For an easy comprehension of the APF approach, its flowchart is shown in Fig. 2. Note that the APF approach is a response-only approach that relies only on measured longitudinal VSs of structures under inspection and is independent of response data of intact structures. If VSs of intact structures are available, a baseline dataset can be built and trained for intelligent damage identification by artificial intelligence algorithms such as deep learning, which can be addressed in some future study. It is also noteworthy that the APF approach is a reference-free approach: vibration frequencies and material and structural parameters of structures can be unknown, making the approach feasible for structures made of not only isotropic materials but also orthotropic materials such as fiber-reinforced composite laminates [45]. However, the APF approach is an offline approach that relies on postprocessing of measured VSs. In contrast, eigen-perturbation techniques that have attracted considerable attention promise to identify structural damage in real time [5], examples being recursive principal component analysis [46] and recursive singular spectrum analysis [47]. Thus, fast measurement and processing of VS data streams with real-time algorithms can be addressed in some future study.

3. Verification of the approach

The capability of the APF approach in identifying damage in a bar is analytically verified in this section. Note that analytical solutions of longitudinal VSs of bars are continuous and noise-free here. For verification of the APF approach, analytical VSs of bars are spatially discretized and Gaussian noise is added to them to simulate environmental noise interference. Consider an undamped bar of length L, which contains a two-sided notch along its length. The bar is divided into three segments by edges of the notch section with lengths L_j $(j = 1, 2, 3)$. Two intact segments are joined by the notch segment with reduced cross-sectional dimensions. Let x be the abscissa and $\zeta = x/L$ be the dimensionless coordinate. Let x_j be the abscissa of the jth change in the cross-section and $\zeta_j = l_j = x_j/L$ be the dimensionless abscissa of x_j. The dimensionless length of the notch is $l_2 - l_1$. Let $\zeta_c = x_c/L$ denote the dimensionless central location of a notch, where x_c is the central location of the notch with the subscript c denoting the center of the notch. Dimensions of the bar with a notch is shown in Fig. 3.

The elastic modulus and mass density of the bar are denoted as E and ρ, respectively, which are assumed to be constant. The cross-sectional area of the jth segment of the bar is A_j, which is assumed to be constant for each segment. A dimensionless parameter $\xi = (H - h)/H$ is used to represent thickness reduction of the notch with H and h denoting thicknesses of intact and notched cross-sections, respectively. An aluminum bar of length 500 mm, width 25 mm, and thickness 6 mm

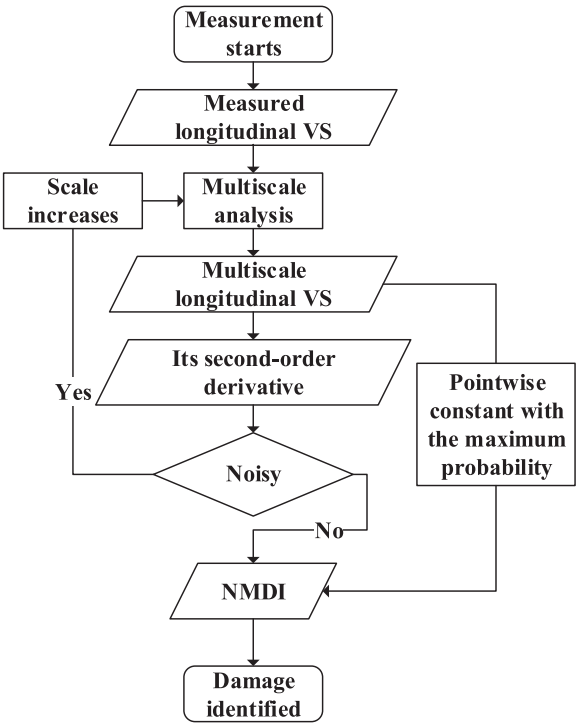

Fig. 2. Flowchart of the APF approach.

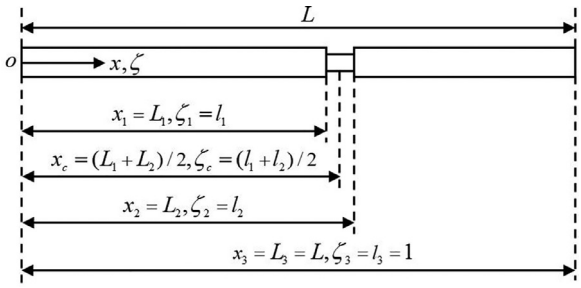

Fig. 3. Dimensions of the bar with a notch.

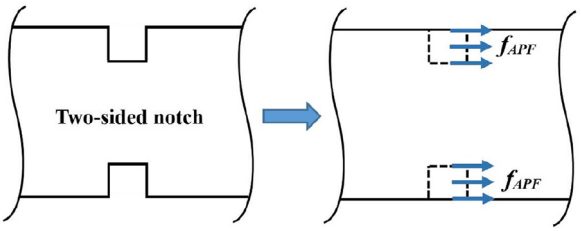

Fig. 4. Schematic of the APF applied on a bar element with a two-sided notch.

is considered as a specimen, whose elastic modulus and mass density are 70 GPa and 2700 kg/m^3, respectively. A two-sided notch with reduced cross-sectional dimensions is introduced by symmetrically reducing the thickness of the specimen from both its top and bottom surfaces throughout its width. Fig. 4 shows a schematic of the APF applied on a bar element with a two-sided notch. Damage Scenarios I-VIII of the specimen are used for verification of the approach, where different vibration frequencies and notch locations and extents are considered, as illustrated in Table 1.

Table 1
Damage Scenarios I-VIII.

Scenario	I	II	III	IV	V	VI	VII	VIII
$l_2 - l_1$	0.2	0.12	0.05	0.05	0.05	0.05	0.05	0.05
ζ_c	0.5	0.5	0.5	0.3	0.4	0.5	0.6	0.7
ξ	0.2	0.15	0.1	0.1	0.1	0.1	0.1	0.1
Frequency (Hz)	4867.9	4931.1	4988.7	1000	2000	3000	4000	5000

3.1. Notch identification using longitudinal MSs

The equation of longitudinal motion of the undamped bar is expressed as [40]

$$E\frac{\partial^2 u_j(x,t)}{\partial x^2} - \rho\frac{\partial^2 u_j(x,t)}{\partial t^2} = 0,\ j = 1,2,3, \tag{19}$$

where u_j is the longitudinal displacement of the jth segment, whose solution can be assumed as

$$u_j(x,t) = U_{M,j}(x)\sin(\omega_n t),\ j = 1,2,3, \tag{20}$$

in which $U_{M,j}(x)$ is the jth segment of the longitudinal MS of the bar associated with its natural frequency ω_n. Substituting Eq. (20) into Eq. (19) yields

$$\frac{\mathrm{d}^2 U_j(x)}{\mathrm{d}x^2} + \frac{\rho}{E}\omega_n^2 U_j(x) = 0. \tag{21}$$

By introducing the dimensionless abscissa $\zeta = x/L$, the general solution to Eq. (21) can be expressed as

$$\begin{aligned} U_{M,1}(\zeta) &= e_{M,1}\cos\eta_{M,1}\zeta + f_{M,1}\sin\eta_{M,1}\zeta, 0 \le \zeta \le l_1,\\ U_{M,2}(\zeta) &= e_{M,2}\cos\eta_{M,2}\zeta + f_{M,2}\sin\eta_{M,2}\zeta, l_1 \le \zeta \le l_2,\\ U_{M,3}(\zeta) &= e_{M,3}\cos\eta_{M,3}\zeta + f_{M,3}\sin\eta_{M,3}\zeta, l_2 \le \zeta \le 1, \end{aligned} \tag{22}$$

where $e_{M,j}$ and $f_{M,j}$, in which $j = 1,2,3$, are constants to be determined by boundary and continuity conditions, and $\eta_{M,j} = L\omega_n\sqrt{\rho_j/E_j}$ is the dimensionless natural frequency of each bar segment. The axial force in a bar segment is $EA_j U_{M,j}{}'(\zeta)$, where a prime denotes differentiation with respect to ζ.

By taking a free-free bar as an example, its boundary conditions at its two ends are

$$U'_{M,1}(\zeta)\big|_{\zeta=0} = 0,\ U'_{M,3}(\zeta)\big|_{\zeta=1} = 0. \tag{23}$$

Continuity conditions of the displacement and axial force at two edges of the notch section, *i.e.*, $\zeta = l_1$ and $\zeta = l_2$, are

$$U_{M,1}(\zeta) = U_{M,2}(\zeta)|_{\zeta=l_1},\ EA_1 U'_{M,1}(\zeta) = EA_2 U'_{M,2}(\zeta)|_{\zeta=l_1}, \tag{24a}$$

and

$$U_{M,2}(\zeta) = U_{M,3}(\zeta)|_{\zeta=l_2},\ EA_2 U'_{M,2}(\zeta) = EA_3 U'_{M,3}(\zeta)|_{\zeta=l_2}, \tag{24b}$$

respectively. Substituting Eq. (22) into Eqs. (23) and (24) yields six homogeneous equations with six unknown constants $e_{M,j}$ and $f_{M,j}$. To obtain a nontrivial solution, the determinant of the coefficient matrix is set to zero, from which natural frequencies of the bar can be solved and $e_{M,j}$ and $f_{M,j}$ can be solved by normalizing MSs with unit maximum absolute values. Accordingly, $U_{M,j}(\zeta)$ can be obtained by Eq. (22).

Following the foregoing procedure, the first MSs of the bar for Scenarios I-III are obtained by Eq. (22). Fig. 5 shows the first MS for Scenario I, which is continuous at locations of notch edges. By Eq. (8), DIs for Scenarios I-III are obtained and shown in Fig. 6, in each of which two discontinuity peaks sharply rise at locations of the notch edges, clearly indicating and locating the notch, whose locations are in good agreement with actual notch edge locations: the identified notches for Scenarios I-III span from ζ=0.4 to 0.6, 0.44 to 0.56, and 0.475 to 0.525, respectively. In addition, Fig. 6 shows that ratios of amplitudes of the DIs for the three scenarios are approximately 2:1.5:1, which are consistent with ratios of thickness reductions of the three notches. This finding corresponds to the inference of Eq. (7) that the amplitude of the APF is proportional to the thickness reduction of the bar in the notch section.

3.2. Notch identification using longitudinal SRSHEs

The equation of longitudinal motion of the jth segment of the undamped bar under the distributed axial harmonic excitation force $f(x,t)$ with the excitation frequency ω that excludes an undamped longitudinal natural frequency of the bar can be expressed as [40]

$$EA_j\frac{\partial^2 u_j(x,t)}{\partial x^2} - \rho A_j\frac{\partial^4 u_j(x,t)}{\partial t^2} = f(x,t),\ j = 1,2,3, \tag{25}$$

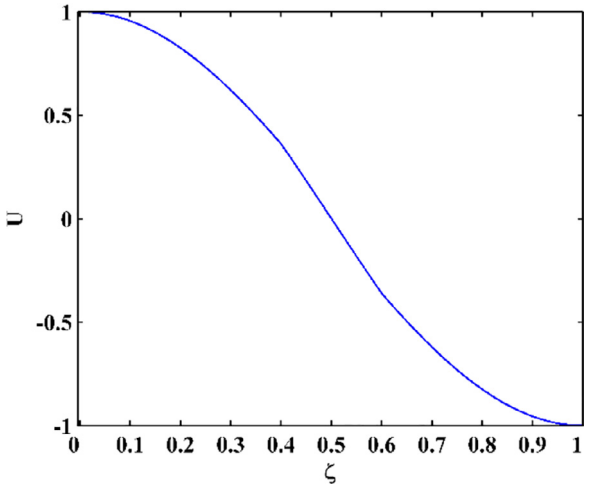

Fig. 5. First MS for Scenario I.

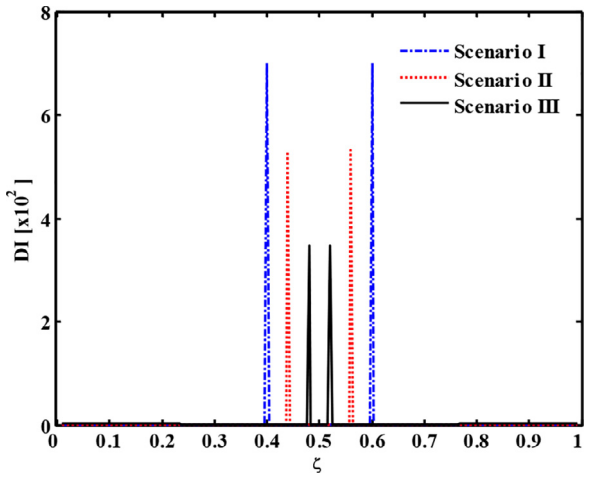

Fig. 6. DIs for Scenarios I-III.

whose solution can be assumed as

$$u_j(x,t) = U_{S,j}(x)\sin(\omega t), \tag{26}$$

where $U_{S,j}(x)$ is the jth segment of the longitudinal SRSHE of the bar associated with the excitation frequency ω.

Consider a pointwise harmonic excitation $f(x,t) = F\sin(\omega t)\delta(L-x)$ with the amplitude F applied at a free end $(x = L)$ of the bar. Since $f(x,t)$ vanishes for $x \in [0, L)$, solutions to $U_{S,j}(x)$ for $x \in [0, L)$ have the same forms as those in Eq. (22):

$$\begin{aligned} U_{S,1}(\zeta) &= e_{S,1}\cos\eta_{S,1}\zeta + f_{S,1}\sin\eta_{S,1}\zeta, 0 \le \zeta \le l_1, \\ U_{S,2}(\zeta) &= e_{S,2}\cos\eta_{S,2}\zeta + f_{S,2}\sin\eta_{S,2}\zeta, l_1 \le \zeta \le l_2, \\ U_{S,3}(\zeta) &= e_{S,3}\cos\eta_{S,3}\zeta + f_{S,3}\sin\eta_{S,3}\zeta, l_2 \le \zeta < 1, \end{aligned} \tag{27}$$

where $e_{S,j}$ and $f_{S,j}$, in which $j = 1, 2, 3$, are constants to be determined by boundary and continuity conditions, $\eta_{S,j} = L\omega\sqrt{\rho_j/E_j}$ are the dimensionless frequency of each bar segment corresponding to the excitation frequency. The axial force in each bar segment is $EA_jU_{S,j}{}'(\zeta)$.

Boundary conditions of the bar with the pointwise harmonic excitation force at $x = L$ are

$$U'_{S,3}(\zeta)\big|_{\zeta=0} = 0,\ U'_{S,3}(\zeta)\Big|_{\zeta=1} = -\frac{F}{EA_3}. \tag{28}$$

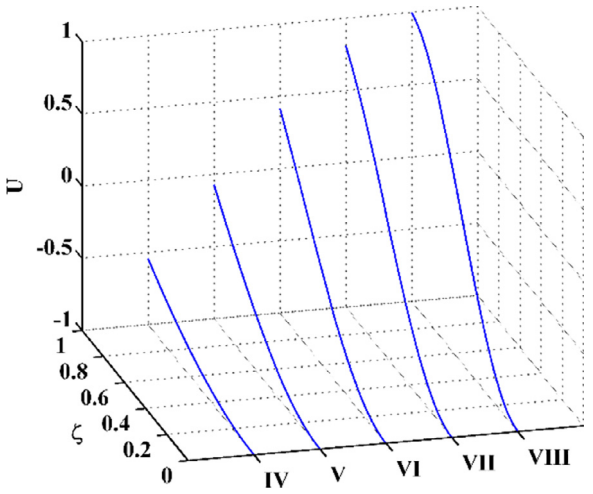

Fig. 7. VSs for Scenarios IV-VIII.

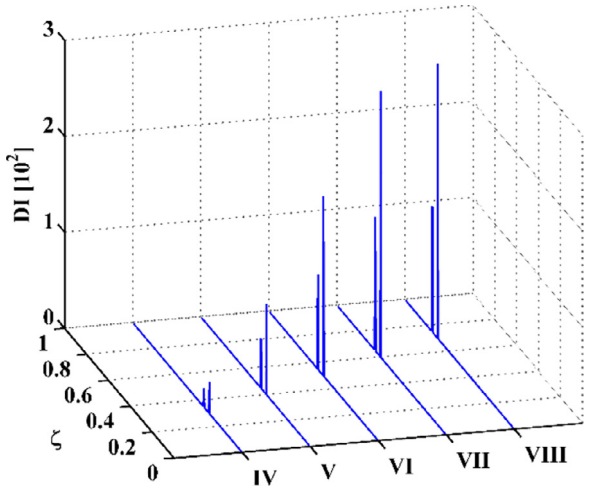

Fig. 8. DIs for Scenarios IV-VIII.

Continuity conditions of the displacement and axial force at two edges of the notch section, *i.e.*, $\zeta = l_1$ and $\zeta = l_2$, are

$$U_{S,1}(\zeta) = U_{S,2}(\zeta)|_{\zeta=l_1},\ EA_1U'_{S,1}(\zeta) = EA_2U'_{S,2}(\zeta)|_{\zeta=l_1}, \tag{29a}$$

and

$$U_{S,2}(\zeta) = U_{S,3}(\zeta)|_{\zeta=l_2},\ EA_2U'_{S,2}(\zeta) = EA_3U'_{S,3}(\zeta)|_{\zeta=l_2}, \tag{29b}$$

respectively. Substituting Eq. (27) into Eqs. (28) and (29) yields six nonhomogeneous equations, from which six unknown constants $e_{S,j}$ and $f_{S,j}$ can be solved by assuming that the pointwise harmonic excitation force has a unit amplitude (1 N). Accordingly, $U_{S,j}(\zeta)$ can be obtained by Eq. (27), which has the same shape with different force amplitudes under the linear vibration assumption.

To verify the feasibility of the proposed approach for a VS with an arbitrary vibration frequency, normalized SRSHEs of the bar with unit maximum amplitudes associated with vibration frequencies of 1000, 2000, 3000, 4000, and 5000 Hz for Scenarios IV-VIII, respectively, are obtained following the foregoing procedure. Correspondingly, for notches with a dimensionless length of 0.05, their dimensionless central locations ζ_c are 0.3, 0.4, 0.5, 0.6, and 0.7, respectively. The SRSHEs are obtained by Eq. (27) and shown in Fig. 7, which are continuous at locations of the notch edges. DIs for Scenarios IV-VIII are obtained by Eq. (8) and shown in Fig. 8. It can be seen from Fig. 8 that at locations of the notch edges in each scenario, two discontinuity peaks in each DI sharply rise to clearly indicate and locate the notch, which correspond to actual locations of the notch edges. Thereby, the approach proposed in this study is feasible for identifying notches using either a MS or a SRSHE with an arbitrary vibration frequency. It is noteworthy that to obtain SRSHEs of the structures under inspection, they need to be excited by single frequencies, which is difficult to achieve for some large-scale structures. Use of VSs under ambient excitations can be addressed in some future study.

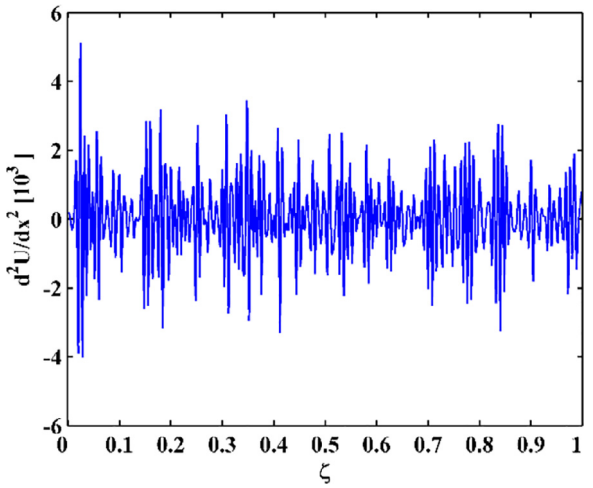

Fig. 9. d^2U/dx^2 in a noisy condition.

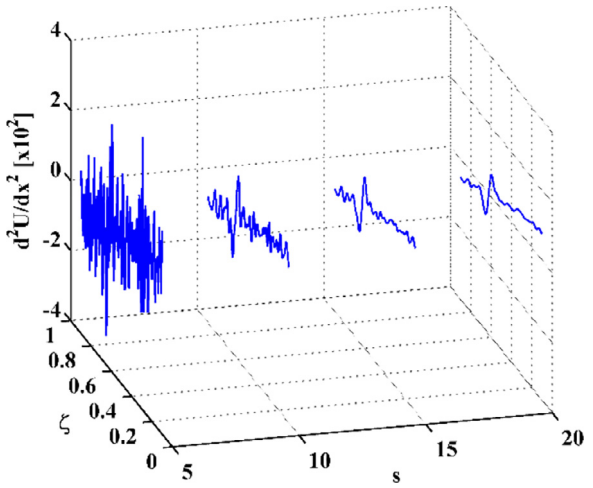

Fig. 10. d^2U_s/dx^2 in a noisy condition.

3.3. Notch identification without knowing material and structural parameters

To simulate a noisy condition, white Gaussian noise of a signal-to-noise ratio (SNR) of 70 dB is individually added to a longitudinal SRSHE at 4900 Hz of a bar whose notch spans from $\zeta = 0.6$ to 0.65, from which d^2U/dx^2 is obtained by Eq. (14) and shown in Fig. 9. It can be seen from Fig. 9 that noise interference dominates d^2U/dx^2 and masks the notch-induced discontinuity peaks. To eliminate noise interference, U is convoluted with the scaled Gaussian window by Eq. (15). By gradually increasing the scale parameter, d^2U_s/dx^2 at scale parameters of 5, 10, 15, and 20 are obtained and shown in Fig. 10, where noise components in U are gradually removed until d^2U_s/dx^2 becomes smooth at the scale parameter of 20.

By substituting U_{20} into Eq. (16), the MDI is obtained and shown in Fig. 11, where two discontinuity peaks in DI_{20} sharply rise, by which occurrence of the notch is clearly manifested and its two edges are located at about $\zeta = 0.6$ and 0.65, corresponding to the actual locations of the notch edges indicated by two vertical lines. When the vibration frequency and material and structural parameters are unknown, the constant λ^2 is evaluated by the normalization strategy to be 38.7 (the exact value of λ^2 can be calculated by $\lambda^2 = \frac{\omega^2\rho^I}{E^I}$ to be 38.1), with which the NMDI is obtained by Eq. (17) and shown in Fig. 12. Similar to discontinuity peaks in Fig. 11, two discontinuity peaks in Fig. 12 clearly indicate and locate the notch. Note that the MDI in Fig. 11 is divided by A^IE^I for comparison with the NMDI in Fig. 12. Thereby, the proposed approach is verified to be effective in damage identification in noisy conditions even when vibration frequencies and material and structural parameters are unknown.

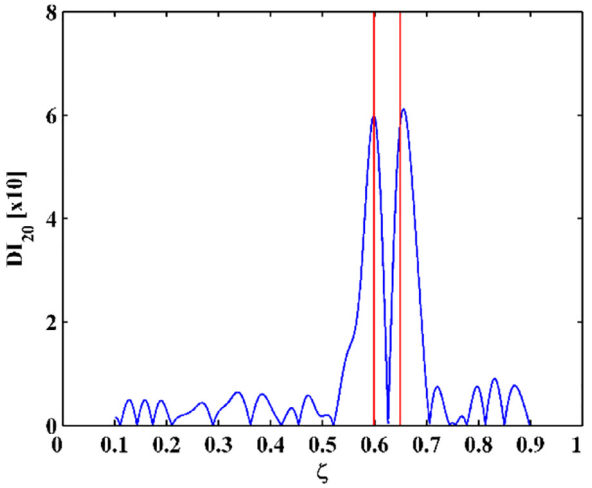

Fig. 11. MDI in a noisy condition.

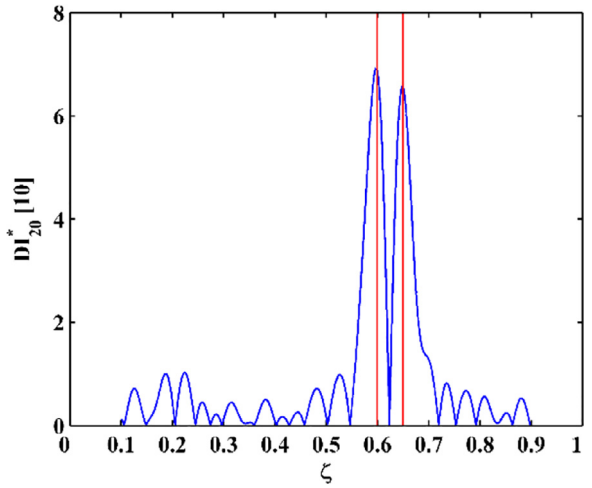

Fig. 12. NMDI in a noisy condition.

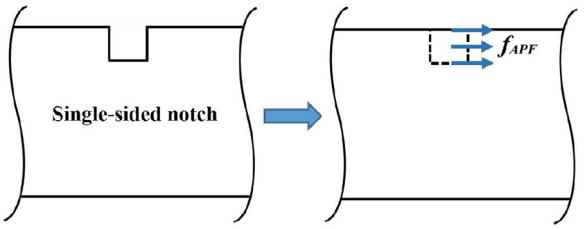

Fig. 13. Schematic of the APF applied on a bar element with a single-sided notch.

3.4. Crack identification in noisy conditions

By considering a bar element with a single-sided notch, the APF is applied on one side of the element, as illustrated in Fig. 13. When the length of the notch is much smaller than dimensions of the bar, the notch can be regarded as a perpendicular single-sided crack. In that situation, the APF is perpendicularly applied along the crack, as illustrated in Fig. 14.

Considering that the analytical bar model bears a crack at $\zeta = 0.4$ with a width of 0.2 mm (dimensionless width of 0.0004) and depth of 0.6 mm (dimensionless reduction in thickness of 0.1); its VS under an axial excitation at 5000 Hz is shown in Fig. 15. By Eq. (8), the DI is obtained and shown in Fig. 16. It can be seen from Fig. 16 that a peak in the DI is

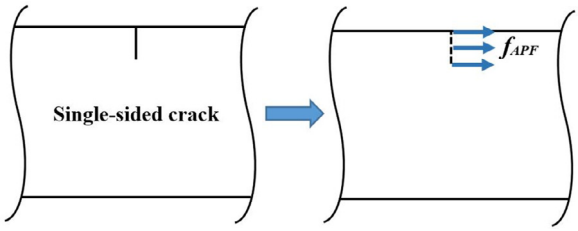

Fig. 14. Schematic of the APF applied on the bar element with a single-sided crack.

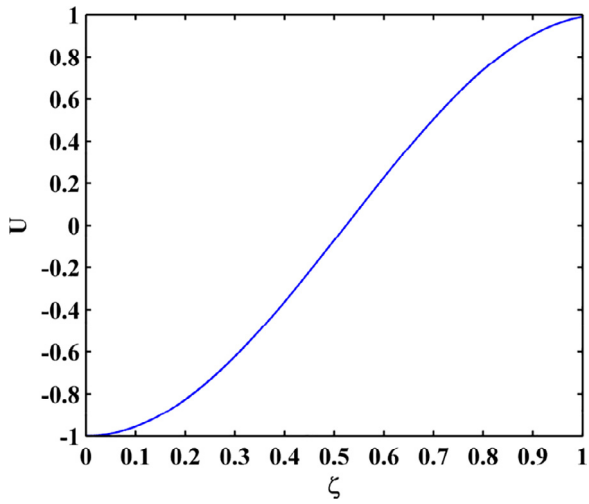

Fig. 15. VS of the bar with the crack.

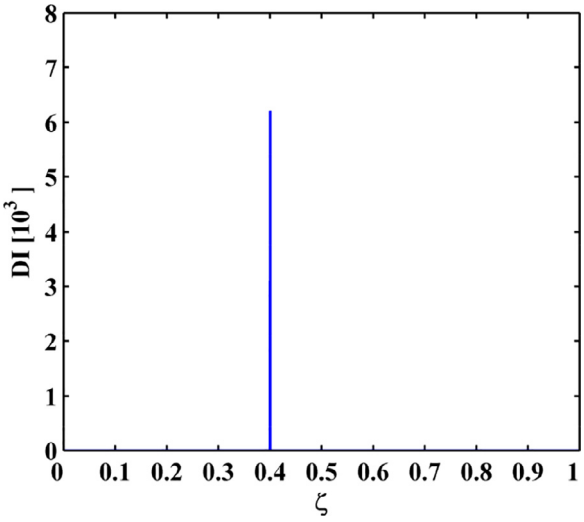

Fig. 16. DI of the bar with the crack.

concentrated at the crack location and values of the DI at undamaged locations vanish. Note that as two edges of the crack are close to each other, two peaks that correspond to the two crack edges merge into one single peak.

To verify the robustness of the NMDI against noise interference, SNRs of VSs decrease from 70 dB to 50 dB and thence to 30 dB. The NMDIs are obtained by Eq. (17) and shown in Fig. 17. For the SNR of 70 dB, it can be seen from Fig. 17(a) that the NMDI with the scale parameter of 25 bears an evident crack-induced peak at the crack location; meanwhile, noise-induced burrs appear in the DI at undamaged locations. For the SNR of 50 dB, it can be seen from Fig. 17(b) that more intense noise interference to the NMDI is suppressed when the scale parameter increases to 30. For the SNR of 30 dB, it can be seen from Fig. 17(c) that although the crack-induced peak in the NMDI can still be identified by increasing the scale parameter to 35,

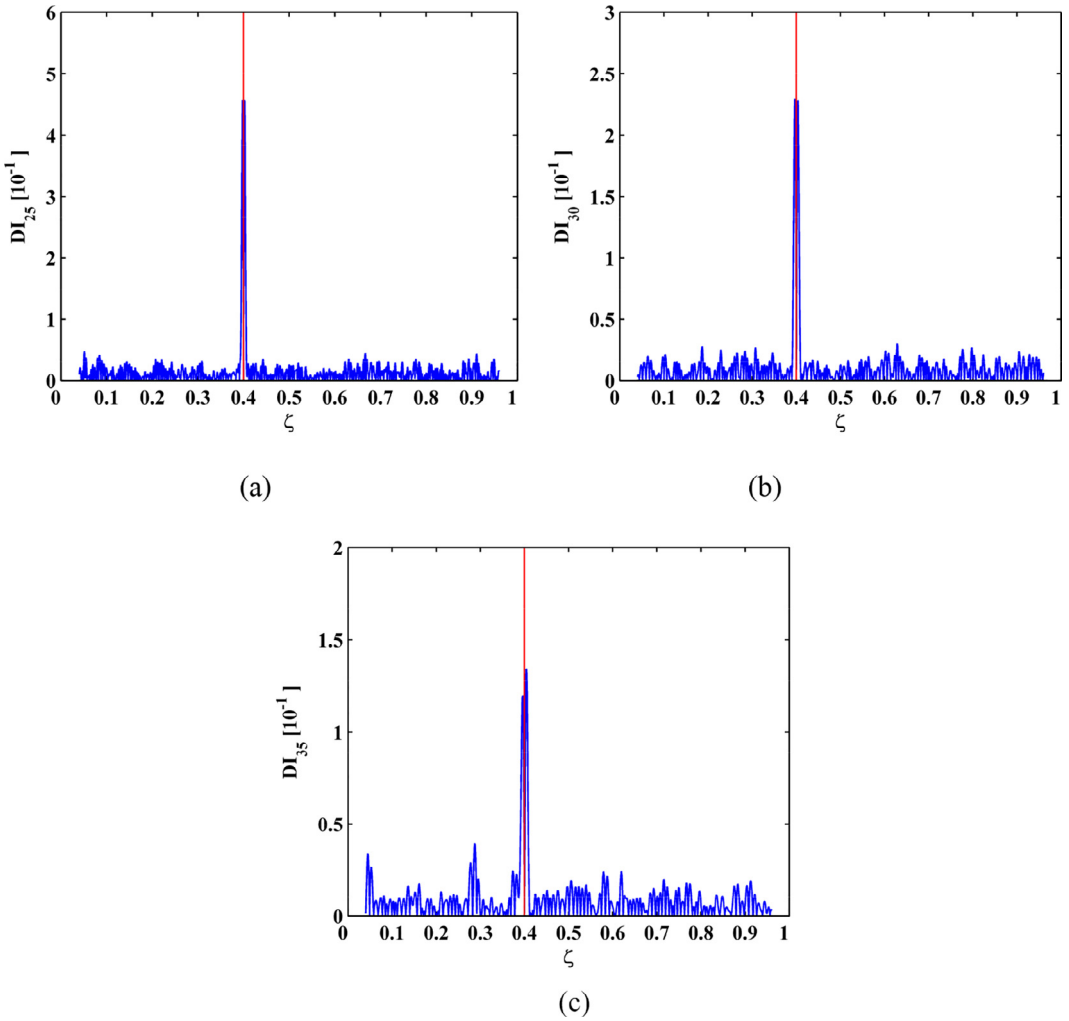

Fig. 17. NMDIs in noisy conditions with SNRs of (a) 70 dB, (b) 50 dB, and (c) 30 dB.

some noise-induced fake peaks with less pronounced amplitudes also appear at undamaged locations. Thus, the SNR of 30 dB can be regarded as the limit of the APF approach for crack identification in this case. Thereby, besides identification of notches, the APF approach is capable of identifying cracks with much smaller widths.

4. Experimental validation

The applicability of the approach is experimentally validated by identifying a two-sided notch in a bar through non-contact vibration measurement using a 3D SLV.

4.1. Experimental specimen and setup

The experimental specimen of an aluminum bar with a two-sided notch is shown in Fig. 18, whose elastic modulus and mass density are 70.5 GPa and 2680 kg/m^3, respectively. The aluminum bar is 475 mm long, 25.4 mm wide, and 6.35 mm thick. The notch with a length of 55 mm is manufactured by symmetrically milling 1.25 mm in the thickness of the specimen from its both top and bottom surfaces throughout its width. Dimensionless reduction in thickness $\xi = (H - h)/H$ of the specimen is about 0.4. To simulate free-free boundary conditions of the bar, it is suspended by four flexible strings that are glued to its four corners of the upper surface; an MB Dynamics Modal 50A electromagnetic shaker is attached to the end of the bar farther away from the notch, as shown in Fig. 18(a). The zoomed-in view of the notch is shown in Fig. 18(b) to display its details. The measurement line, which is indicated by dots in Fig. 18(a) to represent the laser spot moving along it, on one lateral side along the length of the bar is 450 mm in length, whose origin is 2 mm away from its end without excitation applied to it; the notch is 145 through 200 mm away from the origin of the measurement line,

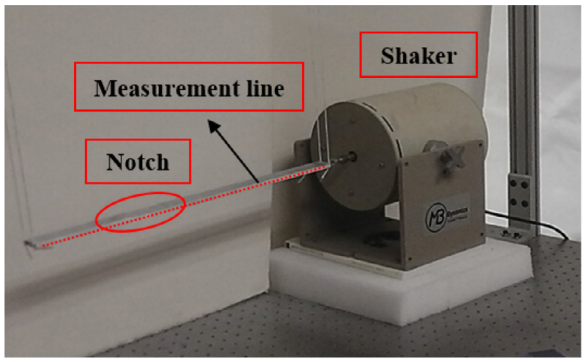

(a)

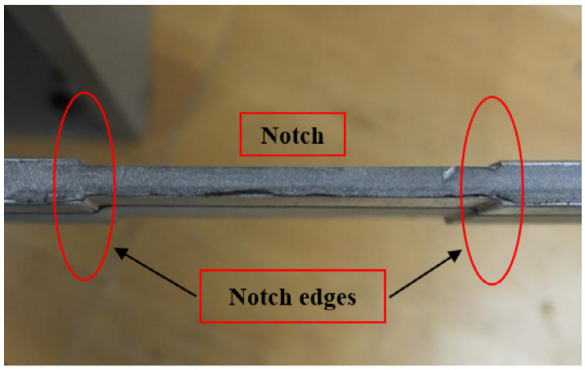

(b)

Fig. 18. (a) Aluminum bar with a two-sided notch, which is excited by an electromagnetic shaker in the axial direction, and (b) the zoomed-in view of the notch.

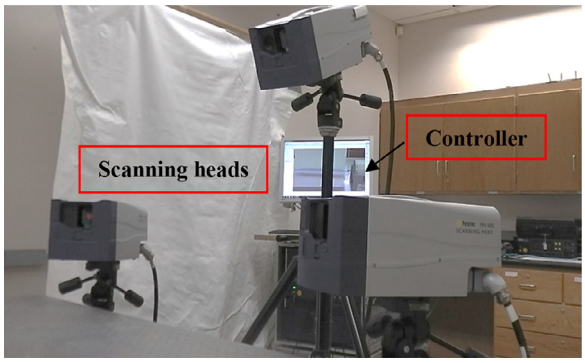

Fig. 19. 3D SLV with three scanning heads and a controller.

whose dimensionless coordinate is ζ =0.322 through 0.444. As the maximum excitation frequency of the shaker is 5000 Hz, and the first undamped longitudinal natural frequency of the bar is estimated to be 4968.6 Hz by the analytical solution in Section 3, the first damped longitudinal natural frequency of the bar cannot be accurately acquired due to the limitation of the shaker. In this restricted case, a SRSHE having a similar shape to that of the first MS is used to validate the applicability of the APF to both MSs and SRSHEs. The shaker produces a harmonic force to excite the bar in the axial direction at 4900 Hz, which is close to the first calculated undamped longitudinal natural frequency of the bar and within the excitation frequency range of the shaker, so that the SRSHE has a similar shape to that of the first MS of the bar. Consequently, the longitudinal SRSHE at 4900 Hz is used in this study to validate the applicability of the proposed approach for damage identification.

The experimental setup of a 3D SLV (Polytec PSV-500-3D) is shown in Fig. 19. Steady-state velocity responses of the bar are acquired by the 3D SLV at 255 uniformly distributed measurement points along the measurement line. Longitudinal

operating deflection shapes (ODSs) of the bar are extracted using LMS Test.Lab 9b's animation module by analyzing averaged cross-power spectra of the measurement points. The real part of the ODS at 4900 Hz is regarded as the longitudinal SRSHE for this lightly-damped bar, since its magnitude is much larger than that of the imaginary part, which leads to a higher SNR [6] that benefits structural damage identification.

4.2. Experimental results

Fig. 20 shows the measured longitudinal SRSHE at 4900 Hz, from which its second-order derivative d^2U/dx^2 is shown in Fig. 21. It can be seen from Fig. 21 that noise components are intensely amplified by differentiation and dominate d^2U/dx^2. As a result, damage-induced discontinuities in d^2U/dx^2 are masked by noise interference and fail to indicate any damage. To eliminate noise interference, U is convoluted with the scaled Gaussian window by Eq. (15). By gradually increasing the scale parameter s to a satisficing level of 50, d^2U_{50}/dx^2 becomes smooth with success in removal of noise interference.

By substituting U_{50} into Eq. (16), the MDI is obtained and shown in Fig. 22, where two sharply rising discontinuity peaks in DI_{50} clearly indicate occurrence of the notch and pinpoint its two edges at about ζ =0.32 and 0.45, which correspond to actual locations of the notch edges indicated by two vertical lines, *i.e.*, x =145 and 200 mm. In a practical scenario, baseline information such as the vibration frequency and material and structural parameters can be unknown. In this case, the constant λ^2 needs to be estimated in a statistical manner, which is evaluated by the normalization strategy to be 36.5 (the exact value of λ^2 can be calculated by $\lambda^2 = \frac{\omega^2 \rho^I}{E^I}$ to be 36.0); consequently, the NMDI is obtained by Eq. (17) and shown in Fig. 23. It can be seen that the NMDI is highly consistent with the MDI: two discontinuity peaks in Fig. 23 clearly indicate and locate the notch and are consistent with the two discontinuity peaks in Fig. 22. Note that the MDI in Fig. 22 is

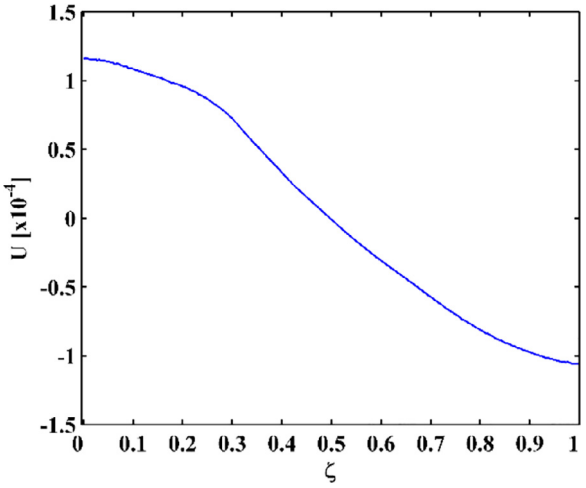

Fig. 20. Measured longitudinal SRSHE.

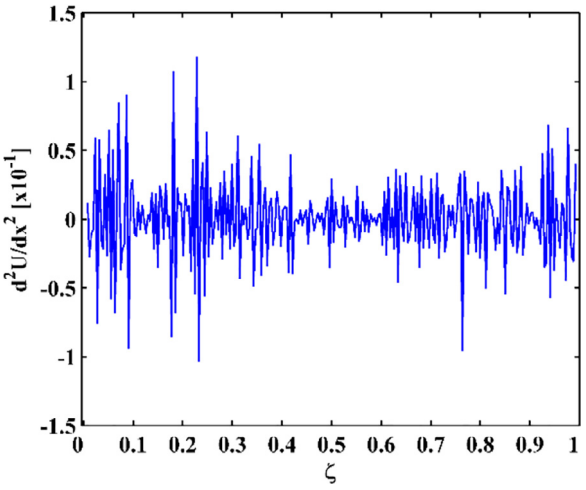

Fig. 21. d^2U/dx^2 for the longitudinal SRSHE.

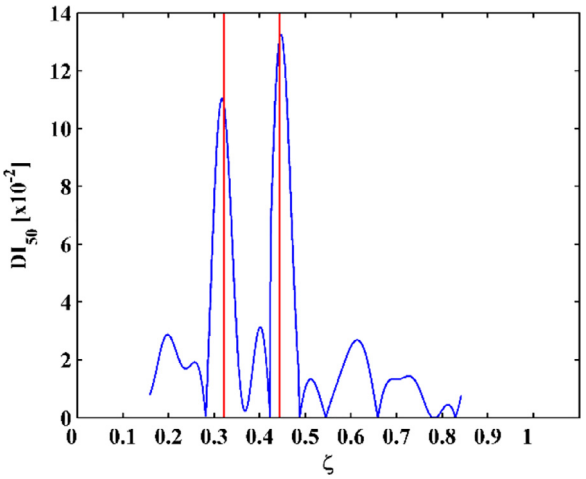

Fig. 22. MDI for the SRSHE.

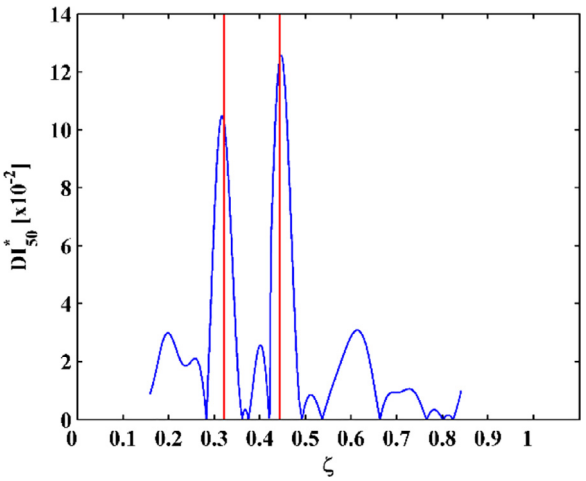

Fig. 23. NMDI for the SRSHE.

divided by $E^I A^I$ for comparison with the NMDI in Fig. 23. Thereby, the APF approach proposed in this study can be applied to damage identification of longitudinally vibrating structures in noisy conditions even though vibration frequencies and material and structural parameters are unknown.

5. Concluding remarks

Among damage identification methods relying on flexural VSs, the TPF approach features high sensitivity to initial damage. However, the TPF approach is inapplicable to some structures governed mainly by tension and not bending, such as cables in a cable-stayed bridge, because bending effects on their flexural vibrations are much smaller compared to their tension effects. In this study, a new concept of APF is formulated using damage-induced perturbation in longitudinal vibration, which forms the basis of a novel damage identification approach for longitudinally vibrating structures. The capability of the approach in identifying damage in longitudinally vibrating structures is analytically verified on bars with two-sided notches and cracks. The applicability of the approach is experimentally validated by identifying a two-sided notch of an aluminum bar through non-contact vibration measurement using a 3D SLV. Some conclusions are as follows.

(1) The APF is concentrated within the damage region only and rapidly attenuates at undamaged locations; meanwhile, discontinuity peaks in the APF sharply rise at damage boundaries, *e.g.*, notch edges. Thereby, the absolute value of the amplitude of the APF can be used as the DI to characterize the occurrence, location, and extent of the damage. The analytical mechanism for having discontinuity peaks in the DI at damage boundaries is explicitly expounded.
(2) To enhance robustness of the DI against noise interference, the region-by-region manner is used to inspect a longitudinal VS by sliding a scaled Gaussian window function along the VS signal, whereby random noise involved in the VS can be averaged. By gradually increasing the scale parameter to a satisficing level, noise components in the VS can be

gradually eliminated; meanwhile, damage-induced discontinuity peaks at damage boundaries are naturally retained to indicate and locate the damage.

(3) Elastic moduli, cross-sectional areas, and mass densities are assumed to be constant in longitudinally vibrating structures under the intact status in this work. To ensure the applicability of the proposed approach to real-world structures under inspection whose material and structural parameters are unknown, a normalization strategy is proposed to evaluate the constant λ^2 in a statistical manner, which is independent of baseline information of the vibration frequency and material and structural parameters.

(4) The APF approach is an offline approach that relies on postprocessing of measured VSs, which can inhibit its applicability for damage identification in real time. Fast measurement and processing of VS data streams with real-time algorithms can be addressed in some future study. On the other hand, to obtain SRSHEs of structures under inspection, they need to be excited by single frequencies, which is difficult to achieve for some large-scale structures. Use of VSs under ambient excitations can be addressed in some future study.

Declaration of Competing Interest

The authors declare that they have no known competing financial interests or personal relationships that could have appeared to influence the work reported in this paper.

CRediT authorship contribution statement

Wei Xu: Conceptualization, Methodology, Software, Validation, Writing - original draft. **Weidong Zhu:** Conceptualization, Methodology, Validation, Funding acquisition, Writing - review & editing. **Zhongqing Su:** Methodology, Funding acquisition. **Maosen Cao:** Methodology, Funding acquisition. **Hao Xu:** Methodology, Funding acquisition.

Acknowledgment

Weidong Zhu is grateful for the support from the National Science Foundation through Grant No. CMMI-1763024. Zhongqing Su, Maosen Cao, and Hao Xu are grateful for the support from the National Natural Science Foundation of China through Grant Nos. 51875492, 11772115, and 12072056, respectively. The authors would also like thank Scott Smith in the Department of Mechanical Engineering at the University of Maryland, Baltimore County for the help on the experimental work.

References

[1] C. Farrar, K. Worden, An introduction to structural health monitoring, Philos. Trans. R. Soc. A-Math. Phys. Eng. Sci. 365 (2007) 303–315.
[2] A.S. Nobari, M.H. Ferri Aliabadi, Vibration-Based Techniques for Damage Detection and Localization in Engineering Structures, World Scientific Publishing, 2018.
[3] T. Kundu, Nonlinear Ultrasonic and Vibro-Acoustical Techniques for Nondestructive Evaluation, Springer, 2019.
[4] A. Bovsunovsky, C. Surace, Non-linearities in the vibrations of elastic structures with a closing crack: a state of the art review, Mech. Syst. Signal Process. 62-63 (2015) 129–148.
[5] C.N. Wong, W.D. Zhu, G.Y. Xu, On an iterative general-order perturbation method for multiple structural damage detection, J. Sound Vib. 273 (1–2) (2004) 363–386.
[6] W. Xu, W.D. Zhu, S. Smith, M. Cao, Structural damage detection using slopes of longitudinal vibration shapes, J. Vib. Acoust. 138 (2016) 345013.
[7] W. Xu, W. Zhu, Y. Xu, M. Cao, A comparative study on structural damage detection using derivatives of laser-measured flexural and longitudinal vibration shapes, J. Nondestr. Eval. 39 (2020) 59.
[8] A. Pandey, M. Biswas, M. Samman, Damage detection from changes in curvature mode shapes, J. Sound Vib. 145 (1991) 321–332.
[9] M. Cao, P. Qiao, Novel Laplacian scheme and multiresolution modal curvatures for structural damage identification, Mech. Syst. Sig. Process. 23 (2009) 1223–1242.
[10] M. Yoon, D. Heider, J. Gillespie Jr., C. Ratcliffe, R. Crane, Local damage detection with the global fitting method using mode shape data in notched beams, J. Nondestr. Eval. 28 (2009) 63–74.
[11] M. Yoon, D. Heider, J. Gillespie Jr., C. Ratcliffe, R. Crane, Local damage detection with the global fitting method using operating deflection shape data, J. Nondestr. Eval. 29 (2010) 25–37.
[12] J. Kim, E. Lee, S. Rahmatalla, H. Eun, Non-baseline damage detection based on the deviation of displacement mode shape data, J. Nondestr. Eval. 32 (2013) 14–24.
[13] Y.F. Xu, W.D. Zhu, J. Liu, Y.M. Shao, Identification of embedded horizontal cracks in beams using measured mode shapes, J. Sound Vib. 333 (2014) 6273–6294.
[14] M. Cao, W. Xu, W. Ren, W. Ostachowicz, G. Sha, L. Pan, A concept of complex-wavelet modal curvature for detecting multiple cracks in beams under noisy conditions, Mech. Syst. Sig. Process. 76-77 (2016) 555–575.
[15] Y.F. Xu, D.M. Chen, W.D. Zhu, Damage identification of beam structures using free response shapes obtained by use of a continuously scanning laser Doppler vibrometer system, Mech. Syst. Sig. Process. 92 (2017) 226–247.
[16] D.M. Chen, Y.F. Xu, W.D. Zhu, Experimental investigation of notch-type damage identification with a curvature-based method by using a continuously scanning laser Doppler vibrometer system, J. Nondestr. Eval. 36 (2017) 38.
[17] S. Cao, H. Ouyang, Robust structural damage detection and localization based on joint approximate diagonalization technique in frequency domain, Smart Mater. Struct. 26 (2017) 015005.
[18] Z. Yang, M. Radzienski, P. Kudela, W. Ostachowicz, Fourier spectral-based modal curvature analysis and its application to damage detection in beams, Mech. Syst. Sig. Process. 84 (2017) 763–781.
[19] Y.F. Xu, D.M. Chen, W.D. Zhu, Modal parameter estimation using free response measured by a continuously scanning laser Doppler vibrometer system with application to structural damage identification, J. Sound Vib. 485 (2020) 115536.
[20] P. Qiao, W. Lestari, M. Shah, J. Wang, Dynamics-based damage detection of composite laminated beams using contact and noncontact measurement systems, J. Compos. Mater. 41 (2007) 1217–1252.

[21] E. Sazonov, P. Klinkhachorn, Optimal spatial sampling interval for damage detection by curvature or strain energy mode shapes, J. Sound Vib. 285 (2005) 783–801.
[22] Z. Shi, S. Law, L. Zhang, Structural damage detection from modal strain energy change, J. Eng. Mech. 126 (2000) 1216–1223.
[23] M. Cao, W. Xu, W. Ostachowicz, Z. Su, Damage identification for beams in noisy conditions based on Teager energy operator-wavelet transform modal curvature, J. Sound Vib. 333 (2014) 1543–1553.
[24] M. Cao, M. Radzieński, W. Xu, W. Ostachowicz, Identification of multiple damage in beams based on robust curvature mode shapes, Mech. Syst. Sig. Process. 46 (2014) 468–480.
[25] W. Xu, M. Cao, K. Ding, M. Radzieński, W. Ostachowicz, Crack identification in CFRP laminated beams using multi-resolution modal Teager–Kaiser energy under noisy environments, Materials 10 (2017) 656.
[26] K. Liew, Q. Wang, Application of wavelet theory for crack identification in structures, J. Eng. Mech. 124 (1998) 152–157.
[27] Q. Wang, X. Deng, Damage detection with spatial wavelets, Int. J. Solids Struct. 36 (1999) 3443–3468.
[28] M. Rucka, K. Wilde, Application of continuous wavelet transform in vibration based damage detection method for beams and plates, J. Sound Vib. 297 (2006) 536–550.
[29] H. Kim, H. Melhem, Damage detection of structures by wavelet analysis, Eng. Struct. 26 (2004) 347–362.
[30] H. Xu, L. Cheng, Z. Su, J. Guyader, Identification of structural damage based on locally perturbed dynamic equilibrium with an application to beam component, J. Sound Vib. 330 (2011) 5963–5981.
[31] M. Cao, L. Cheng, Z. Su, H. Xu, A multi-scale pseudo-force model in wavelet domain for identification of damage in structural components, Mech. Syst. Sig. Process. 28 (2012) 638–659.
[32] M. Cao, Z. Su, L. Cheng, H. Xu, A multi-scale pseudo-force model for characterization of damage in beam components with unknown material and structural parameters, J. Sound Vib. 332 (2013) 5566–5583.
[33] H. Xu, Z. Su, L. Cheng, J. Guyader, P. Hamelin, Reconstructing interfacial force distribution for identification of multi-debonding in steel-reinforced concrete structures using noncontact laser vibrometry, Struct. Health Monit. 12 (5-6) (2013) 507–521.
[34] H. Xu, Z. Su, L. Cheng, J. Guyader, A “pseudo-excitation” approach for structural damage identification: from “strong” to “weak” modality, J. Sound Vib. 337 (2015) 181–198.
[35] H. Xu, Z. Su, L. Cheng, J. Guyader, On a hybrid use of structural vibration signatures for damage identification: a virtual vibration deflection (VVD) method, J. Vib. Control 23 (4) (2017) 615–631.
[36] H. Xu, B. Lu, Z. Su, L. Cheng, Statistical enhancement of a dynamic equilibrium-based damage identification strategy: theory and experimental validation, J. Sound Vib. 351 (2015) 236–250.
[37] C. Zhang, L. Cheng, H. Xu, J. Qiu, Structural damage detection based on virtual element boundary measurement, J. Sound Vib. 372 (2016) 133–146.
[38] C. Zhang, H. Ji, J. Qiu, L. Cheng, W. Yao, Y. Wu, A local specific stiffness identification method based on a multi-scale “weak” formulation, Mech. Syst. Sig. Process. 140 (2020) 106650.
[39] C. Pezerat, J.L. Guyader, Two inverse methods for localization of external sources exciting a beam, Acta Acust. 3 (1995) 1–10.
[40] W. Weaver Jr, S. Timoshenko, D. Young, Vibration Problems in Engineering, John Wiley & Sons, 1990.
[41] A. Leissa, M. Qatu, Vibration of Continuous Systems, McGraw Hill, 2011.
[42] S. Mallat, A Wavelet Tour of Signal Processing, Academic Press, 2008.
[43] J. Yang, S. Lin, H. Huang, L. Zhou, An adaptive extended Kalman filter for structural damage identification, Struct. Control Health Monit. 13 (4) (2006) 849–867.
[44] D. Roy, G. Rao, Stochastic Dynamics, Filtering and Optimization, Cambridge University Press, 2017.
[45] M. Cao, Z. Su, H. Xu, M. Radzieński, W. Xu, W. Ostachowicz, A novel damage characterization approach for laminated composites in the absence of material and structural information, Mech. Syst. Sig. Process. 143 (2020) 106831.
[46] M. Krishnan, B. Bhowmik, A. Tiwari, B. Hazra, Online damage detection using recursive principal component analysis and recursive condition indicators, Smart Mater. Struct. 26 (8) (2017) 085017.
[47] B. Bhowmik, M. Krishnan, B. Hazra, V. Pakrashi, Real time unified single and multi-channel structural damage detection using recursive singular spectrum analysis, Struct. Health Monit. 18 (2) (2018) 563–589.